# MIMO-Control of a Flexible Rotor with Active Magnetic Bearing

**Chunsheng Wei[1,a], Dirk Söffker[2,b]**
[1] Chair of Dynamics and Control, University of Duisburg-Essen
Lotharstr. 1-21, 47057 Duisburg, Germany
[2] Chair of Dynamics and Control, University of Duisburg-Essen
Lotharstr. 1-21, 47057 Duisburg, Germany
[a]chunsheng.wei@uni-due.de, [b]soeffker@uni-due.de

**Abstract:** The paper presents a comparison of different selected MIMO (Multi Input – Multi Output)-control algorithms applied to a test rotor supported by magnetic bearings in the lateral direction. Here, the contribution is focused on the lateral direction. The rotor is considered as flexible, correspondingly, a FE-model is created, and digital controllers are employed. Moreover, a challenge of controlling the rotors of turbocompressors is to take into account the effects of the fluid forces, which destabilize the first forward mode shape in high pressure applications.
The simulation results are compared with measured data for validation purposes.

## I Introduction

Due to their advantages in comparison to conventional bearings, active magnetic bearings (AMB) have been applied to various rotor systems. For an AMB system, the inherent negative stiffness causes instability of the open loop of the system; therefore, a feedback control loop is employed to stabilize the rotor system. So the controller design becomes a central task for designing the AMB system.

Different control methods are successfully applied to controlling of magnetic bearing systems. The classical PID control method [1] is widely used in AMB systems due to their structure and transparent design. Most of industry AMB systems are controlled by PID-like controllers including also low-pass filter. Nowadays, rotor systems become more and more complex (because of higher energy density, higher speed, more complex rotor structure, etc.), thus it becomes difficult for the PID controller to handle the existing control problems of modern AMB systems. Motivated by this situation, modern control methods have been employed to AMB systems. An optimal method (LQ controller) [2] is used to obtain optimal (high performance) solution concerning control energy and control error. A drawback of these methods is that the robustness properties are not explicitly taken into account and that all states need to be used for feedback (therefore, an observer becomes necessary). Robust control methods ($H_\infty$ controller [3], μ-synthesis, etc.) are developed to cover up some drawbacks of LQ method, focusing on both performance and robustness of the controlled system. Here weighting functions are involved to design the transfer functions of the controlled system in order to achieve the desired performance and robustness.

In this paper, three control methods are designed and compared for a magnetic bearing

supported rotor system. First two PID controllers are employed based on root locus oriented design to control the parallel mode and the tilting mode of the rotor, separately. The second approach is based on LQ design; third, a $H_\infty$ controller is developed. This paper is organized as follows: Section II introduces the models of the rotor system and the magnetic bearing system. In section III the controller design is focused, here the three methods are explained. In section IV, simulations are performed and results are compared. Experimental results are used to validate the control methods in section V. Finally, summary is given in section VI.

## II Modeling

A magnetic bearing-rotor system includes rotor system, sensors, analog-to-digital converters (AD-converters), controller, digital-to-analog converters (DA-converters), amplifiers, and actuators. At first modeling of the rotor system will be discussed; secondly the model of the magnetic bearing system is given. The sensors are taken as proportional transfer elements of second order ($PT_2$) with an eigenfrequency out of the sampling region of the system. The Pulse-Width-Modulation (PWM) amplifiers are employed in the test rig. Current control configuration is chosen, so the amplifiers can be modeled as part of actuators and treated by proportional behavior. The AD-converters and DA-converters are considered by constant gains, denoted by ADG and DAG, respectively.

**Rotor System.** The discretized model of the rotor (fig. 1) is modeled with 18 nodes and totally 72 DoFs (each node possesses 4 DoFs, i.e. translation and rotation in x- and y-plane). The equations of motion result to

$$M\ddot{q} + (D + \Omega G)\dot{q} + Kq = Fw,$$
$$y = Cq,$$

with

M: Mass matrix, D: Damping matrix (proportional damping D = αK),
G: Gyroscopic matrix, K: Stiffness matrix,
F: Input matrix, q: Displacement vector, $q = [q_1^T, q_2^T, q_3^T \cdots q_{18}^T]^T$, $q_i^T = [x_i, y_i, \alpha_i, \beta_i]$,
y: Measured nodes, C: Output matrix (corresponding to sensor nodes)
Ω: Rotational speed, and w: Input force.

The equations of motion are transformed into state-space representation using the state vector $x_r$ by

$$\dot{x}_r = A_r x_r + B_r u_r,$$

and

$$y_r = C_r x_r,$$

where

$$A_r = \begin{bmatrix} 0 & I \\ -M\backslash K & -M\backslash(D + \Omega G) \end{bmatrix}, \qquad B_r = \begin{bmatrix} 0 \\ M\backslash F \end{bmatrix},$$

$$C_r = \begin{bmatrix} C & 0 \end{bmatrix}, \quad \text{and} \quad y_r = y,$$

with the system matrix $A_r$ of order 144×144, the input matrix $B_r$ of order 144×4, and the output matrix $C_r$ of order 4×144.

The state-space model will be used for controller design. The eigenmodes of the rotor are shown in fig. 2. It is known that the eigenmodes and eigenfrequency of a rotor system are speed dependent; the eigenmodes of the system in fig. 2 are displayed for the rotational speed of 2000 [rpm], consisting of the two rigid modes and the first two bending modes. The second bending mode will not be taken into account due to experimental restrictions (sampling rate), so the dynamics only up to the first bending mode is considered for controller design. For the PID controller design, only the 4 rigid modes are used.

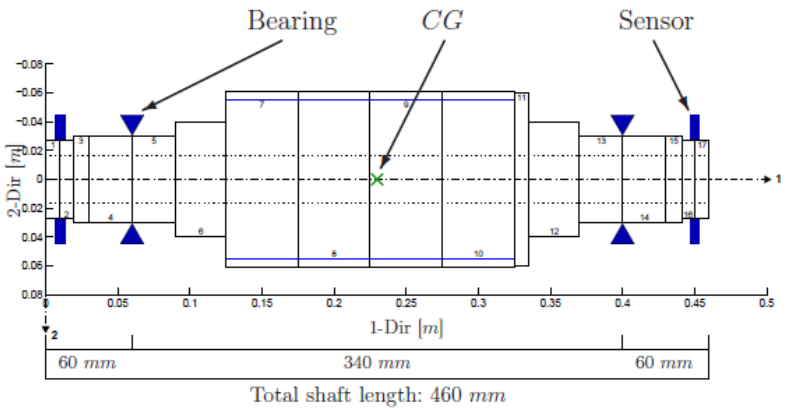


Figure 1: Discretized rotor model

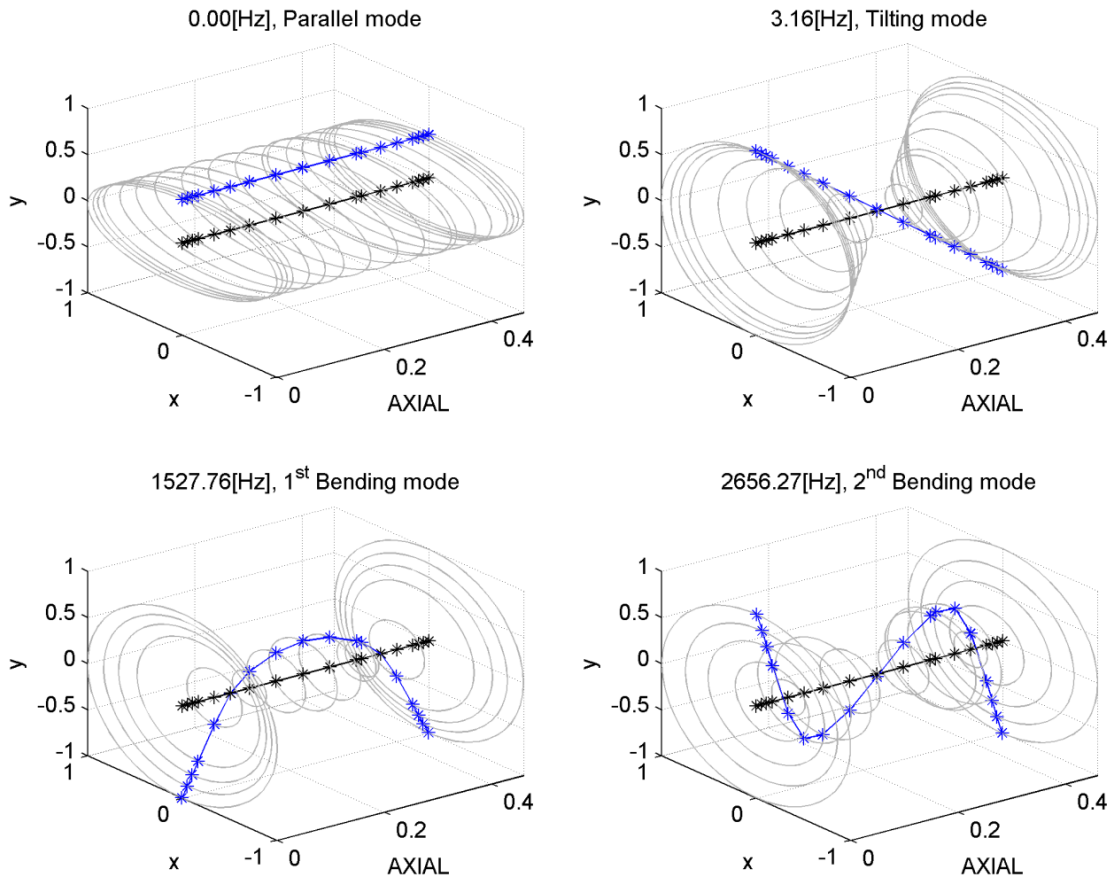


Figure 2: Eigenmodes of the rotor system at rotational speed of 2000 [rpm]

**Magnetic Bearing Model.** According to the available test rig, the differential drive configuration as shown in fig. 3 is employed to linearize the force-current relation of the actuator. In order to achieve current control, an additional underlying current controller (P controller) is used by feedback of the measured current of the magnet coils. The whole actuator system [4] including magnets, amplifiers, and the underlying current controllers, can be represented in state space form by,

$$\dot{x}_m = A_m x_m + B_m u_m ,$$

and

$$y_m = C_m x_m ,$$

with the displacement of the bearing nodes and the control current as inputs $u_m$ of order 8×1, magnetic forces as outputs $y_m$ of order 4×1, the state vector $x_m$ of order 4×1, system matrix $A_m$ of order 4×4, input matrix $B_m$ of order 4×8, and outputs matrix $C_m$ of order 4×4.

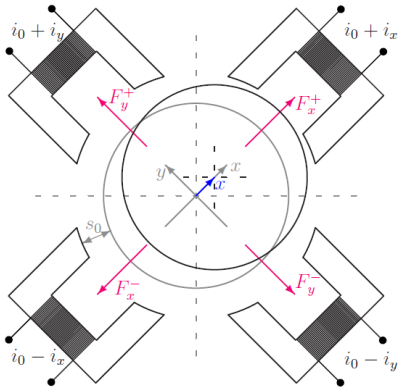


Figure 3: Actuator geometry (differential drive configuration)

A simplified model neglecting the actuator dynamics can be written as

$$f_m = k_s x + k_i i \,,$$

where $k_s$ denotes the negative bearing stiffness, and $k_i$ the force/current factor. This model will be used for designing the PID controller given in section III.

Table 1: Numerical parameters of the system design

| | Units | Value |
|---|---|---|
| Mass of the rotor | [Kg] | 11 |
| Length of the rotor | [m] | 0.46 |
| Distance between the two bearing | [m] | 0.34 |
| Polar moment of inertia | [kg m²] | 0.0174 |
| Transverse moment of inertia | [kg m²] | 0.1834 |
| Negative bearing stiffness $k_s$ | [N/m] | -6.2e6 |
| Force/current factor $k_i$ | [N/A] | 350 |
| Air gap $s_0$ | [mm] | 0.2 |
| AD-converter gain ADG | [-] | 10240000 |
| DA-converter gain DAG | [-] | 0.0039 |

## III Controller Design

By controlling the magnetic bearing system, three methods are carried out in the paper.

**PID Controller.** PID controller, due to its easy to use structure and design transparency, is usually the first choice to control an AMB system and is employed in most of the AMBs in industry application. A root-loci design procedure is performed to obtain the PID controller gains.

Firstly, the rigid rotor model in sensor-coordinates is transformed into center of mass coordinates with a transformation matrix. It can be written in x-plane as

$$x_c = \frac{1}{2}(x_l + x_r),$$
$$\alpha = (x_r - x_l),$$

yielding to

$$\begin{bmatrix} x_c \\ \alpha \end{bmatrix} = \underbrace{\begin{bmatrix} 1/2 & 1/2 \\ -1 & 1 \end{bmatrix}}_{\text{transformation matrix}} \begin{bmatrix} x_l \\ x_r \end{bmatrix}.$$

The indexes l, r, and c denote left sensor node, right sensor node, and rotor midspan node, respectively.

The transformation allows the decoupling of the “parallel” modes and the “tilting” modes. Two PD controllers (with low-pass filters) are designed by using root locus method to control the “parallel” modes and the “tilting” modes. The root loci of both close-loops are shown in fig. 4. Furthermore, adding an integrator term to each controller gives the final PID controllers as

$$C_p = k_p \frac{s + \omega_p}{\left(\left(\frac{s}{\alpha_p \omega_p}\right)^2 + 2\xi\left(\frac{s}{\alpha_p \omega_p}\right) + 1\right)^2 {\omega_p}^2} + \frac{K_I}{s},$$

$$C_t = k_t \frac{s + \omega_t}{\left(\left(\frac{s}{\alpha_t \omega_t}\right)^2 + 2\xi\left(\frac{s}{\alpha_t \omega_t}\right) + 1\right)^2 {\omega_t}^2} + \frac{K_I}{s}.$$

The introduced PID-design is a typical design procedure similar to these used in industry application [4]. The parameters are given in table 2. The controllers stabilize the bearing-rotor system even with sampling delay introduced by zero-order-hold elements. The control current (as controller output) has to be transformed back into bearing-coordinate to be fed into the actuator.

Table 2: PID controller parameters

| Parameter | | |
|---|---|---|
| Parallel-mode Controller $C_p$ | $k_p$ | 700 |
| | $\omega_p$ | 168 [Hz] |
| | $\alpha_p$ | 7 |
| Tilting-mode Controller $C_t$ | $k_t$ | 0.5 |
| | $\omega_t$ | 215 [Hz] |
| | $\alpha_t$ | 6 |
| | | 0.5 |
| | $K_I$ | 1.5 |

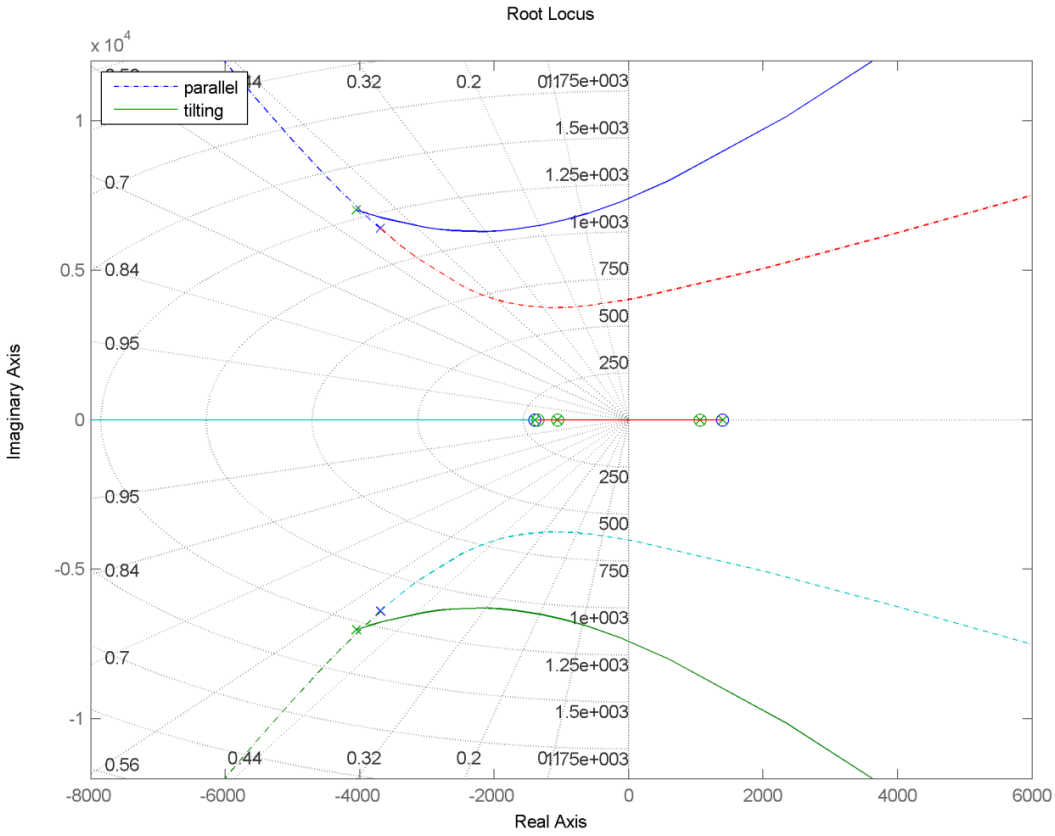


Figure 4: Root loci of the parallel and tilting closed-loop

**LQ Controller.** A LQ controller is designed under the assumption that all states of the controlled system are available for feedback. In this paper, a LQ controller [7] with integrator part to eliminate the static error, is introduced. The structure of the closed-loop system is given in fig. 5. The state-space model can be written as

$$\begin{bmatrix}\dot{x}\\ \dot{e}\end{bmatrix} = (A_I - B_I K_I)\begin{bmatrix}x\\ e\end{bmatrix} + \begin{bmatrix}Nn\\ 0\end{bmatrix} n + E_I w\,,$$

$$y = C_I \begin{bmatrix}x\\ e\end{bmatrix}.$$

with

$$A_I = \begin{bmatrix}A & 0\\ C & 0\end{bmatrix},\quad B_I = \begin{bmatrix}B\\ 0\end{bmatrix},\quad E_I = \begin{bmatrix}0\\ -I\end{bmatrix},\quad C_I = [C \quad 0],\quad \text{and } K_I = [K \quad K_e]\,.$$

It should be noticed, that the feedback matrix contains two parts, i.e. K corresponding to the states of the controlled system and $K_e$ to the integrator part. Disturbances (e.g. gravity, unbalance forces) can be introduced into the system by a disturbance input matrix Nn as shown in fig. 5.

To select the weighting matrices Q and R, vibration energy proportional weighting is used [5], i.e. the weighting matrices are diagonal with their elements

$Q_{ii}$ = 1/maximum acceptable value of $x_i^2$ , i = 1..n ,

$R_{ii}$ = 1/maximum acceptable value of $u_j^2$ , j = 1..4 .

The weighting matrix Q is structured according to the state vector

$$x_g = \begin{bmatrix} x \\ e \end{bmatrix} = [[\text{sensor part}]^T, [\text{rotor part}]^T, [\text{actuator part}]^T, [\text{integrator part}]^T]^T ,$$

as

$$Q = diag\left(\left[\overbrace{[\ldots, 10^{-8}, \ldots]}^{\text{sensor part}}, \left[\underbrace{[\ldots, 10^{8}, \ldots]}_{\substack{\text{displacement} \\ \text{ofrotor nodes}}}, \underbrace{[\ldots, 1, \ldots]}_{\substack{\text{velocity of} \\ \text{rotor nodes}}}\right], \overbrace{[\ldots, 0.0086, \ldots]}^{\text{actuator part}}, \underbrace{[\ldots, 1.5 \times 10^{5}, \ldots]}_{\text{integrator part}}\right]\right),$$

and

$$R = diag([1,1,1,1]) \times 5.96 \times 10^{-8} .$$

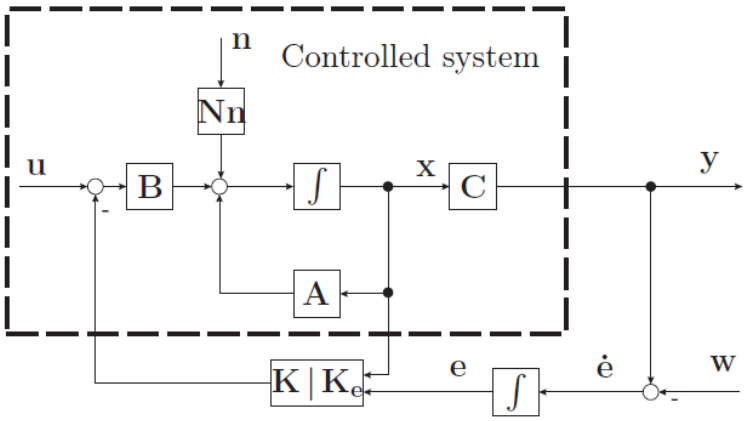


Figure 5: LQ controller with integrator part

**$H_\infty$ Controller.** The $H_\infty$ controller is obtained to be quite similar to a PID controller by using the scheme (fig. 6) from [6].

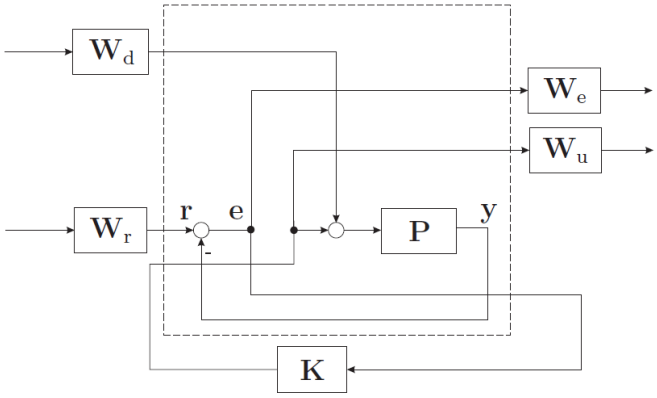


Figure 6: Block diagram of the closed-loop with H∞ controller K and plant P

In order to obtain a controller of low order, the order of the plant is reduced to 28 using balanced model truncation. The parameters to calculate the controller are given in table 3 and the singular value of the resulted controller is shown in fig. 7.

Table 3: Parameters of H∞ controller

| Variable | Parameter |
|---|---|
| $W_e$ | $\frac{10^4}{6}\frac{(s+80)}{(s+10^{-7})}$ |
| $W_u$ | $\frac{1}{7}\frac{(\frac{s}{4800})^2+0.6(\frac{s}{4800})+1)}{(\frac{s}{4800\times 20})^2+1.4(\frac{s}{4800\times 20})+1)}$ |
| $W_r$ | $2\times 10^{-4}$ |
| $W_d$ | 2 |

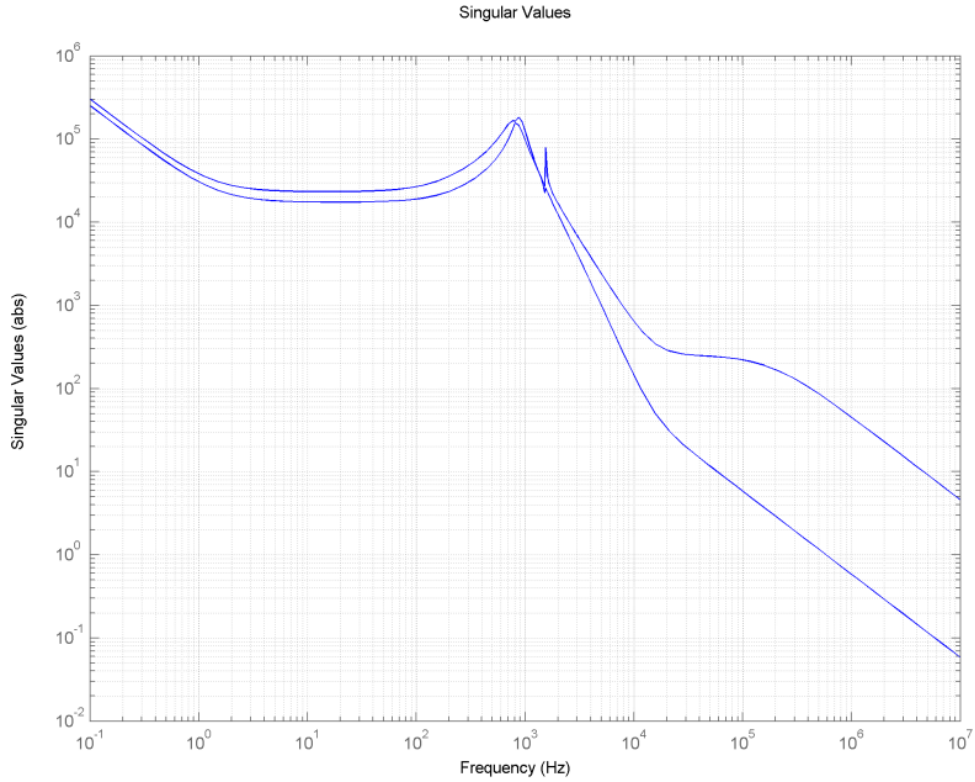


Figure 7: Singular value of the $H_\infty$ controller

## IV Simulation Results

In this section simulation results from the three controllers are shown and compared. Therefore a step response (starting at t = 0.05 [sec], amplitude ≈ 5 [µm]) is calculated to compare the results of the controlled output. Gravity (g = 9.81 [m/s²]) and unbalance ($U_g = 3.5 \times 10^{-5}$ [kg m], at the speed of 2000 [rpm]) are introduced as unknown disturbance.

**Time History.** To compare the three controllers, the dynamical behavior is compared. As shown in fig. 8, obviously, the LQ controller gives the best results. Due to the gravity, the rotor goes down at first and reaches a minimum. This minimum is about -16 [µm] for the system with $H_\infty$ controller,

-12 [µm] for the one with PID controller, and about -0.05 [µm] for the one with LQ controller. Meanwhile the LQ controller compensates the gravity very fast compared with the other both controllers. It can also be seen in fig. 8.b) that the LQ controller leads to the smallest overshoot. Another advantage given by LQ controller is that the controller can compensate the harmonic disturbance (unbalance force) completely.

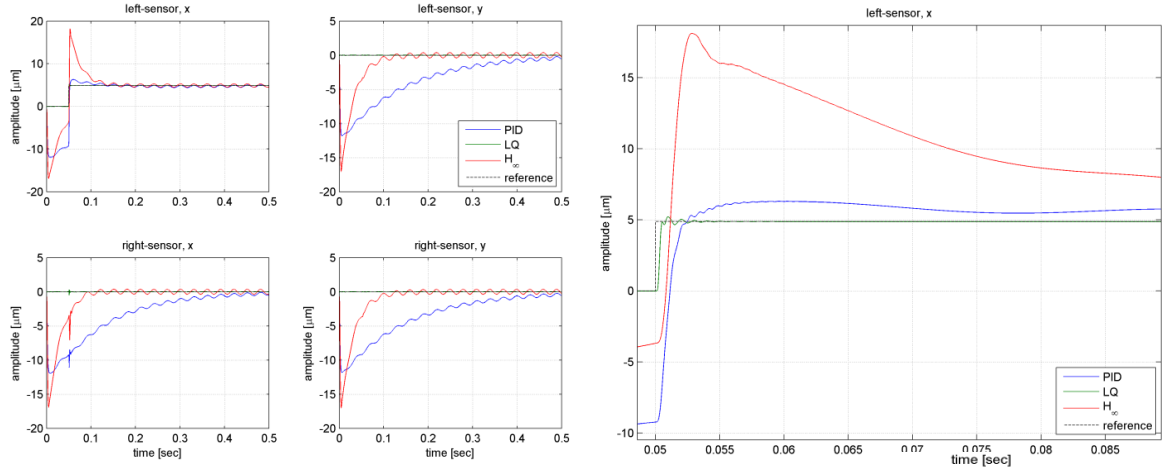


Figure 8: a) Vibration of the sensor nodes; b) Vibration of the left sensor node at t = 0.05 sec

The magnetic force and coil currents from the left magnetic bearing in x-direction are shown in fig. 9. The advantages of the LQ controller mentioned above, come at the cost of the strong changing (peak in fig. 9) of the coil current. In order to follow a step function (step value: about 5 [µm]) reference, the LQ controller results in a peak (about 1 [A]) of coin current, which can lead to actuator

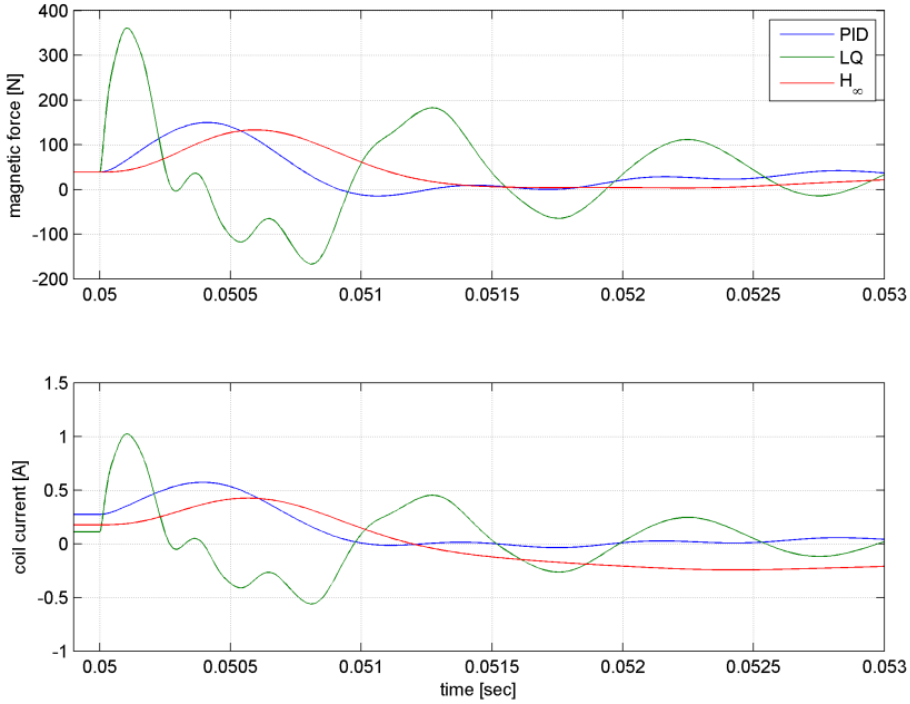


Figure 9: Magnetic force and coil currents of the left magnetic bearing (x-direction)

problems. Similar to the coil current, a peak is noticed in the time history of the magnetic force. These peaks may not be accept-able since it can result in serious problems in practice

due to the existence of the nonlinearity.

**Systematic Comparison of the Behaviors.** In this section, the controller design parameters are varied to examine the structural control behavior of controllers. For the PID and $H_\infty$ controller, the static gains are changed, i.e. the set of controllers can be written as

$$K_i = \alpha_i K, \qquad \alpha = [\alpha_1, \alpha_2, \alpha_3, \alpha_4, \alpha_5] = [0.90, 0.95, 1.00, 1.05, 1.10] .$$

For the LQ controller, the weighting matrix Q is multiplied with a set of parameters $\beta_i$,

$$Q_i = \beta_i Q, \qquad \beta = [\beta_1, \beta_2, \beta_3, \beta_4, \beta_5] = [0.01, 0.05, 0.1, 0.5, 1] .$$

The same simulation is carried out for the three sets of controllers. In order to realize a systematic comparison of the results, the error is calculated in terms of the sum of integral of square of the error, the control effort in terms of the sum of integral of square of the control current, the energy of the rotor in terms of the sum of integral of square of each rotor state, and the energy of the magnetic actuator in terms of the sum of the integral of square of each actuator state i.e.

| | | | |
|---|---|---|---|
| Control effort | $\sum_{i=1}^{4} \int u_i^2 dt$ , | Energy of the rotor (144 states) | $\sum_{r=1}^{144} \int x_r^2 dt$ , |
| Error | $\sum_{i=1}^{4} \int e_i^2 dt$ , | Energy of the actuator | $\sum_{m=1}^{4} \int x_m^2 dt$ . |

The results are shown in fig. 10. The LQ controllers achieve the best results with the lowest control efforts. Since the $H_\infty$ controller is a PID-like controller, it leads to the same trend (with regarding to the control effort and the error) as the PID controller as illustrated in fig. 10.

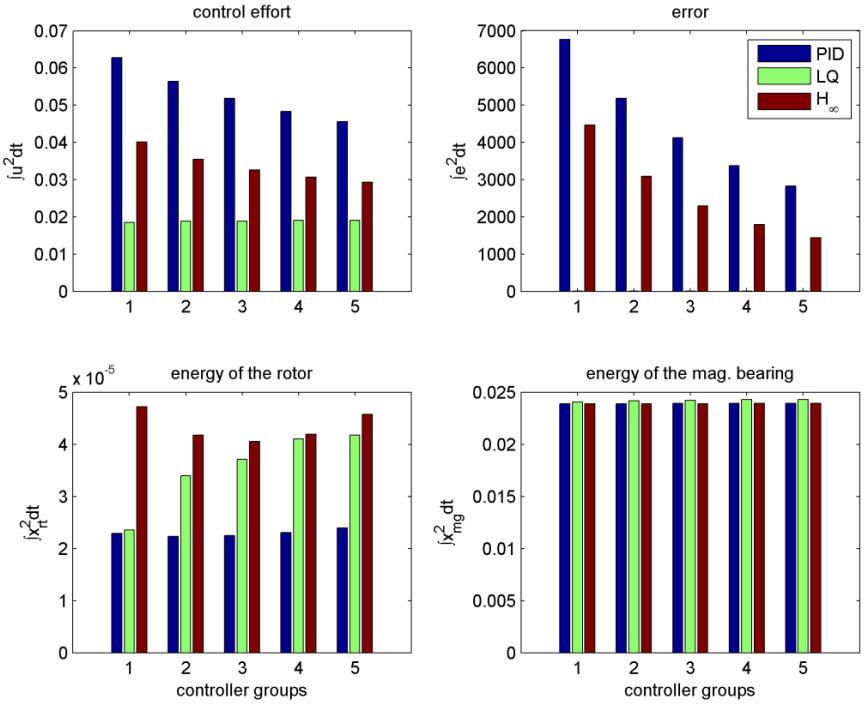


Figure 10: Comparison of the three types of the controllers

**Fluid Forces Influence.** In turbomachines, several types of seal designs, such as labyrinth seals, hole-pattern seals, honeycomb seals, etc. are used, in order to reduce the leakage of working lubricating fluids through the interface between rotor and stator. As a consequence, fluid forces appear, whose behavior strongly depends on the type of seals, pressure difference across the seals and the fluid's density within the seals [8]. The fluid forces may have a strong effect onto the rotordynamic response and stability.

To examine the effect of the fluid force, a simple fluid force model is introduced to the rotor system, which is a function of the displacement of the rotor midspan node. The resulting fluid force is acting again on this rotor midspan node. As a simplest example, the force model is considered by introducing a cross-coupled stiffness matrix, i.e.

$$K_f = \begin{bmatrix} 0 & k_{xy} \\ -k_{xy} & 0 \end{bmatrix}.$$

By varying the coefficient $k_{xy}$ from 1 [N/μm] to 20 [N/μm], a set of simulations is performed to check the stability boundary of the system. The results show that the $H_\infty$ controller can ensure a stable system behavior up to $k_{xy}$ = 5 [N/μm], the PID controller achieve a stable system behavior up to $k_{xy}$ = 9 [N/μm]. The best result can be obtained by using the LQ controller, which leads to a stable system behavior when $k_{xy} \leq 20$ [N/μm]. The simulation results are shown in fig. 11. It is noticeable that due to the existence of the fluid forces the controller takes a while (the chattering region in fig. 11) to compensate the fluid forces and

then the rotor reaches a smooth vibration state.

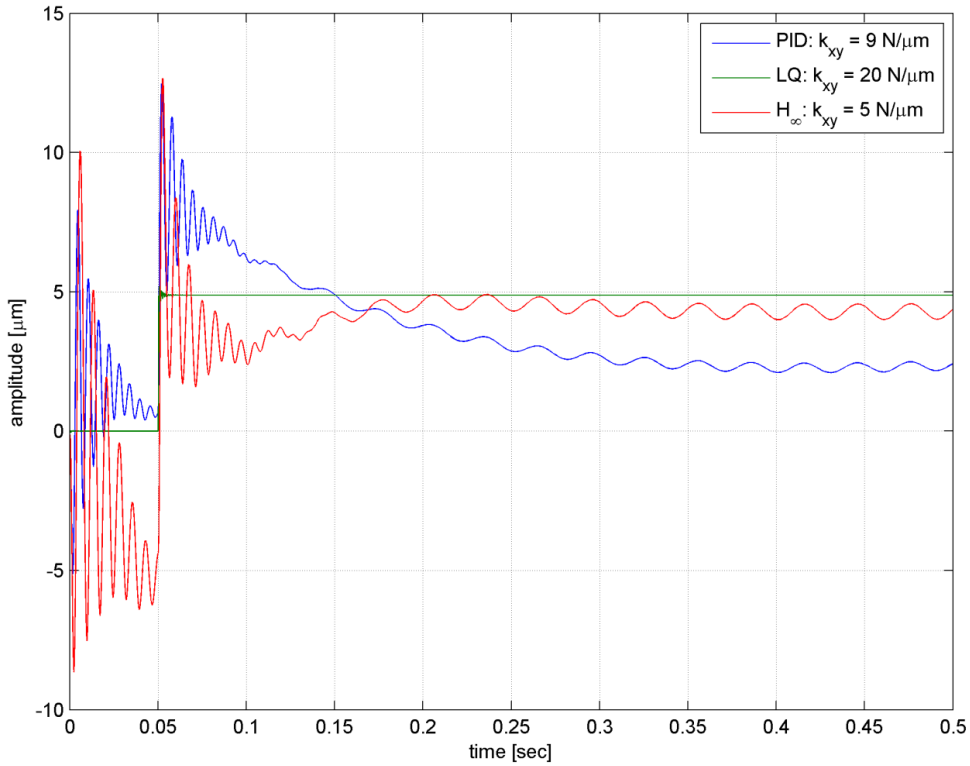


Figure 11: Influence of the fluid forces

## V Experimental Results

In this section experimental results (step response, final value = 50 [DSP] (digitized number)) is presented to verify the control performance. Due to hardware limitations, only the PID controller is implemented in the AMB system and the measured signal will be compared with the obtained simulation results as shown in fig. 11. The simulation results match the experimental result well, although the measured result has a larger overshoot than the simulation one.

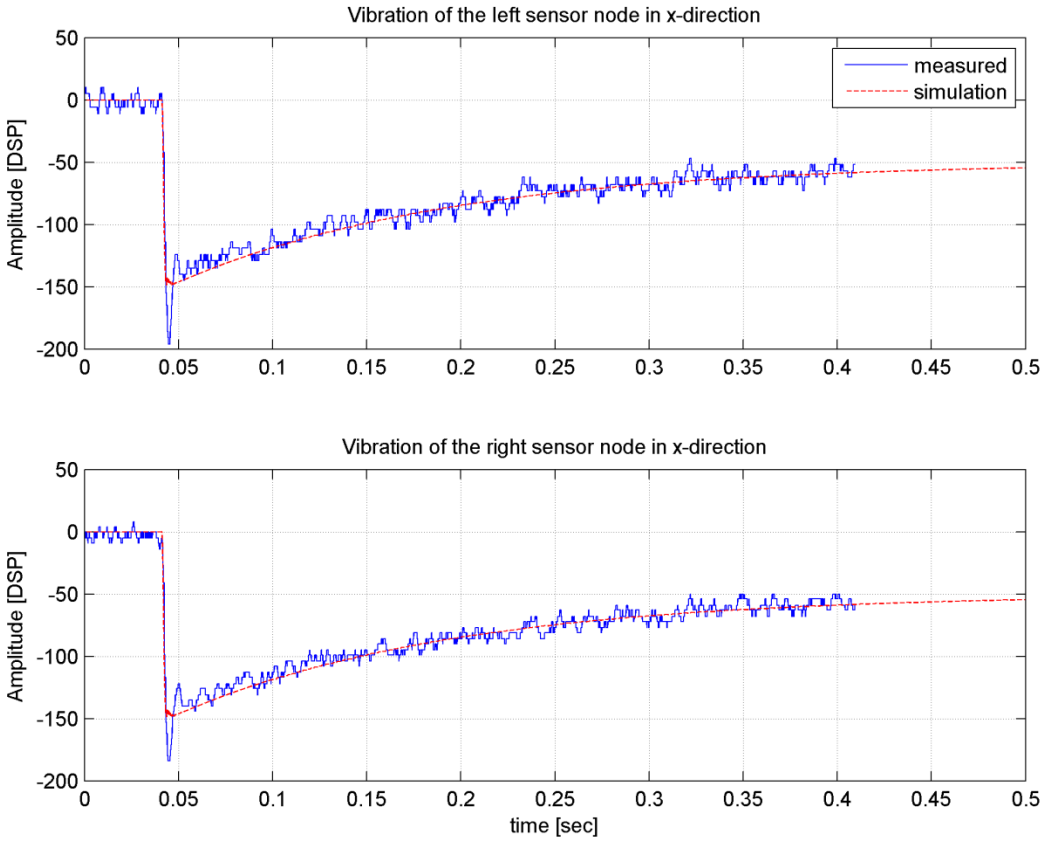


Figure 11: Comparison of experimental and simulation results for PID controller

## VI Summery

Modeling of a rotor system and of related magnetic bearing system is briefly introduced. Three controllers (PID, LQ, $H_\infty$) are designed to control the bearing-rotor MIMO system. Simulations are carried out and the results are systematically compared. Especially, the aspects of control effort, error, and energy of the system are also considered to evaluate the controllers. The LQ controller approach shows structurally the best results. To realize the LQ control, however, the states of the system need to be estimated through an observer. This may lead to a degradation of the obtained very good system behavior. The PID controller is implemented in the real system and the results agree with the measured signal.

## References

[1] B. Polajžer, J. Ritonjak, G. Štumberger, D. Dolinar, J.-P. Lecointe: Decentralized PI/PD position c ontrol for active magnetic bearings, Electrical Engineering, Volume 89, Number 1 / October (200 6), p. 53-59

[2] Rafał Piotr Jastrzębski, Riku Pöllänen: Centralized optimal position control for active magnetic bea rings: comparison with decentralized control, Electrical Engineering, Volume 91, Number 2 / Augu st (2009) p. 101-104

[3] Hiroki Seto, Toru Namerikawa: H∞ DIA Control of a Magnetic Bearing Considering Rotor Unbal ance, LDIA (2005), p. 419-422

[4] Gerhard Schweitzer, Eric H. Maslen, et al.: Magnetic bearings: Theory, Design, and Application to

Rotating Machinery, Springer-Verlag (2009), p. 115-120 & 361-365
[5] Gene F. Franklin, et al.: Feedback control of dynamic systems, Prentice Hall (2005), p. 537
[6] Jan Lunze: Regelungstechnik 2: Mehrgrößensysteme, Digitale Regelung, Springer-Verlag (2008), p. 279-328
[7] Ulrich Schönhoff, Rainer Nordmann: A H∞-weighting scheme for PID-like motion control, Proceed ings of the 2002 IEEE International Conference on Control Applications (2002)
[8] Dara Childs: Turbomachinery rotordynamics: Phenomena modeling, and analysis, John Wiley & So ns, Inc. (1993), p. 290